13,12

Surface morphology and structural properties of GaTe crystals after ion-plasma treatment

© S.P. Zimin[1,2], I.I. Amirov[1], M.S. Tivanov[3], N.N. Kolesnikov[4], O.V. Korolik[3], L.S. Lyashenko[3], D.V. Zhyhulin[5], L.A. Mazaletskiy[2,1], S.V. Vasilev[1], O.V. Savenko[2]

[1] Valiev Institute of Physics and Technology of RAS, Yaroslavl Branch, Yaroslavl, Russia
[2] Demidov State University, Yaroslavl, Russia
[3] Belarussian State University, Minsk, Belarus
[4] Osipyan Institute of Solid State Physics RAS, Chernogolovka, Russia
[5] „Belmicroanaliz" State Center, „INTEGRAL" JSC — „INTEGRAL" Holding Managing Company, Minsk, Belarus

E-mail: zimin@uniyar.ac.ru

Received February 21, 2023
Revised February 21, 2023
Accepted March 1, 2023

The effect of ion-plasma treatment on the physical properties of the surface of GaTe crystals is investigated. Gallium telluride crystals were grown by vertical zone melting under the pressure of an inert argon gas of 10.0 MPa at a temperature of 1000°C and a zone displacement velocity of 9 mm/hr. The treatment was carried out in argon plasma in a high-density low-pressure radio frequency (RF) inductively coupled plasma reactor at an argon ion energy of 100−200 eV for 15−120 s. Using scanning electron microscopy methods, it was shown that the formation of nano- and submicron structures of various architectures (nanohillocks, nanocones, droplet structures) occurred on the surface during processing. It is shown that the sputtering processes are accompanied by enrichment of the near-surface layer with metal atoms and a decrease in oxygen content. The formation of nano- and submicron gallium droplets on the surface has been proved by X-ray diffractometry. The analysis of the Raman scattering spectra showed a decrease in the oxide phases of tellurium after plasma treatment. It is established that modification of the GaTe surface leads to suppression of specular optical reflection in the range of 0.4−6.2 eV.

Keywords: gallium telluride, ion-plasma treatment, nanostructures, X-ray diffractometry, Raman scattering, reflection spectra.

DOI: 10.21883/PSS.2023.04.56012.21

1. Introduction

Gallium telluride (GaTe) has an important position among A^3B^6 semiconductors. Due to its unique properties, this material is widely used for the development of electronic and optoelectronic devices. Gallium telluride is a layered semiconductor [1], it can be easily formed in 2D structures [2–6], has energy diagram with a direct band gap [7–9], can exist in various structural modifications [10–13], has an explicit anisotropy of properties [8,14–16]. These and other properties allow for the use of crystals, films and 2D structures (nanosheets, nanoflakes) of GaTe for the development of photodetectors and solar cells [17,18], transistors and phototransistors [19–21], electronic and photonic elements [22–24], photocatalysis devices [25,26], lithium-ion cells [27], etc.

Currently, along with the extensive study of low-dimensional 2D systems, comprehensive investigations are being conducted in the field of formation and use of 1D objects on the basis of gallium telluride. First results of GaTe nanowires development have been described in [28]. The authors have used the chemical vapor deposition method to synthesize gallium telluride nanowires on silicon substrates with gold islands, which further allowed forming field-effect transistors and flexible photodetectors on the produced low-dimensional 1D objects. Properties of pseudo-1D structures based on gallium telluride are described in [29]. The authors of [25,30] have suggested to use formed GaTe nanofilaments to develop photodetectors with a broadened spectral range and to use 1D structures as active photocatalysts. In [31] the possibility has been shown to grow gallium telluride nanofilaments with a high structural perfection on Si/SiO_2 substrates by means of chemical vapor deposition method without additional metal-catalyst. The analysis of these studies shows the relevance of new approaches to the formation of nanoscale GaTe structures and to the development of non-trivial low-dimensional structures on the surface of gallium telluride crystals and films.

It is known [32] that the method of ion-plasma treatment allows for effective modification of solid surfaces and bring them to nanostructuring. Our studies [33–36] have shown

examples of successful formation of different kinds of nanostructures (nanofilaments, nanorods, nanocones, etc.) with ion-plasma treatment of crystals and films of various semiconductors (PbS, PbTe, PbSe, $Pb_{1-x}Sn_xTe$, $Cu(In,Ga)Se_2$, $Cu_{2-x}Se$, In_2S_3, etc.). The purpose of this study is to investigate the possibility of GaTe crystal surface nanostructuring with the treatment in argon plasma.

2. Experimental part

Gallium telluride single-crystals have been grown by the method of vertical zone-melting under an inert gas (argon) pressure of 10.0 MPa at a temperature of 1000°C and a zone-travel rate of 9 mm/hr. Details of the process and properties of the produced GaTe crystals are described in [10]. The ingot has been split cleaved perpendicularly to the axis of growth into plates with a thickness of about 1 mm. The plate surfaces have been nanostructured in a reactor of high-density argon plasma of low-pressure high-frequency induction discharge (13.56 MHz). The treatment modes were as follows: argon flowrate was 20 sccm, working pressure in the reactor was 0.14 Pa, HF-power on the inductor was 800 W, HF-bias power on the aluminum substrate holder was 125 and 250 W. The average energy (E_i) of Ar^+ ions defined by the HF-power bias was ~ 100 eV and ~ 200 eV, respectively. The ion current density was $5.2\,mA \cdot cm^{-2}$. The duration of ion-plasma treatment (t) was in the range of 15–120 s. The temperature of sample surface was dependent on the energy of ions and the time of treatment, and achieved ~ 500 K when argon ions with an energy of 200 eV were used for 30 s [33].

The surface morphology was studied by scanning electron microscopy (SEM) using Supra 40 (Carl Zeiss) and S-4800 (Hitachi) units in the mode of secondary electron recording. The local chemical analysis and element mapping were carried out using INCA Energy (Oxford Instruments) and Quantex 200 (Bruker) attached units for energy dispersive X-ray (EDX) analysis. The X-ray diffraction studies were performed using an ARL X'tra (Switzerland) diffractometer for Cu K_α radiation.

The Raman scattering (RS) spectra were measured by a Nanofinder HE (LOTIS TII) spectrometer with confocal microscope. The excitation was implemented by a solid-state laser in continuous mode with a wavelength of 532 nm and an optical power of $\sim 60\,\mu$W. The laser radiation was focused onto the sample surface into a spot with a diameter of $\sim 0.6\,\mu$m. The backscattered light was dispersed by a $600\,mm^{-1}$ diffraction grating, which allowed for having a spectral resolution of not worse than $3\,cm^{-1}$.

The specular optical reflection spectra were recorded by a Photon RT (EssentOptics) spectrophotometer. The reflection spectra are obtained with a spectral resolution of not worse than 5 nm in a wavelength range of 200–3000 nm in an unpolarized light with an incident angle on the sample surface of 8°. The size of optical emission beam on the surface under study was about $4.5 \times 4.5\,mm^2$.

3. Results and discussion

3.1. Surface morphology

The surface morphology of gallium telluride crystals in their initial state is shown in Fig. 1, *a*. The cleaved surfaces of GaTe had a condition of mirror with a weakly manifested nanorelief. The processes of ion-plasma treatment with argon ions with an energy of 100 or 200 eV resulted in a significant modification of the surface, related in the general case to both the selective sputtering of gallium telluride and the different behavior of redeposition of chemical elements onto the surface. The sputtering rates of gallium telluride crystals determined on the basis of measurement of heights of the etching steps under the mask were 1.6 ± 0.4 nm/s for 100 eV and 7.8 ± 0.2 nm/s for 200 eV. The resulted sputtering rates are comparable with the sputtering rates of lead chalcogenide crystals and films sputtering and exceed this parameter for known semiconductor materials (Si, InN, GaN, InSb, GaAs, etc.) for similar conditions of sputtering [33]. One of possible causes of the relatively high sputtering rates of GaTe is the layered structure of the material with weak Van der Waals interaction between the layers.

The variation of ion-plasma sputtering conditions in the range of ion energy of 100–200 eV and process time in the range of 15–120 s has shown that the observed pattern of surface morphology can be described within three typical situations: nanohillocks (changes of *type A*, Fig. 1, *b*), nanocones (changes of *type B*, Fig. 1, *c*), drops (changes of *type C*, Fig. 1, *d*). In the case of bombardment by argon ions with an energy of 100 eV at $t = 30$–120 s the nanorelief of the surface became more explicit as compared with the initial state (Fig. 1, *b*), heights of the horns increased up to 40 nm, local areas with lateral dimensions of up to 60 nm started to form on the surface. In the case of treatment by argon ions with an energy of 200 eV for 15–45 s an ensemble of nanocones formed on the surface (Fig. 1, *c*). Heights of these nanocones were as high as 50 nm, the surface density was in the range of $(0.8–3) \cdot 10^{10}\,cm^{-2}$. If the conditions of $E_i = 200$ eV, $t = 45$–120 s were realized, structures in the form of large semispherical drops with lateral dimensions of 100–500 nm appeared on the surface of GaTe crystals (Fig. 1, *d*). Nanostructures with nanodrops on their tops with a diameter of up to 100 nm were arranged between the above-mentioned large drops. To find out the composition of the structures with nanodrops, the architecture of these objects was SEM-studied on the vertical cleavage of the crystal. Fig. 2 shows typical image of the cleavage where dark area corresponds to the crystal body. It follows from the analysis of images that the lower part of the formed structures has a cone shape with a height of up to 200 nm with a quasispherical drop in its upper part.

3.2. Chemical composition of the surface

The investigation of the chemical composition of GaTe crystals in the initial state by EDX method has shown that

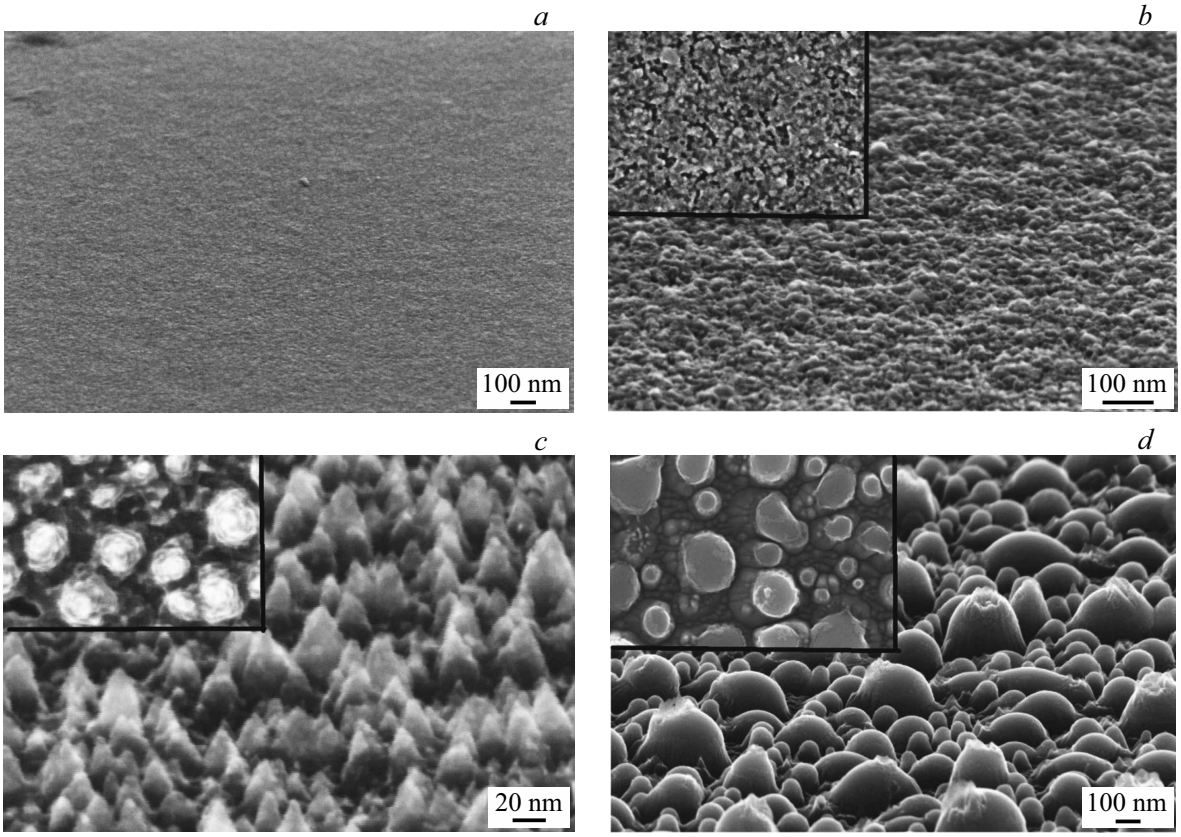

Figure 1. SEM-images of the surface of GaTe crystals after different kinds of treatment. *a* — initial state; *b* — treatment with 100 eV, 120 s; *c* — treatment with 200 eV, 45 s; *d* — treatment with 200 eV, 60 s. The angle of recording is 70°, the inserts show images without sample tilt.

The ratio of chemical elements in the near-surface region of GaTe crystals in the initial state and after the plasma treatment

Surface state	Ga/Te	Ga/Te at tilt	Content of oxygen, at.%
Initial state	1.04−1.12	1.02−1.11	44−53
type A: nanohillocks	1.22−1.70	1.94−2.02	12−28
type B: nanocones	1.52−1.78	1.96−2.19	5−15
type C: drops	2.07−2.19	2.26−2.37	1−3

the ratio of atomic concentrations of gallium and tellurium for the studied crystals in different points of measurement is within the range of 1.04−1.12. In addition, in the near-surface layers the presence of oxygen atoms was noted (44−53 at.%), which was related to the known active oxidizing processes on the gallium telluride surface [26]. The ion-plasma treatment in various modes resulted in changes in the ratio of chemical elements of metal and chalcogen in the near-surface layer. These changes were dependent on the occurred surface modification and are reflected in the table. The composition of elements has been determined in two variants. Due to the fact that the area of EDX analysis covers the surface and a part of body of the sample, along with the standard recording without sample tilt an additional recording was performed with a tilt of 70° that allowed reducing the contribution from the volume. The oxygen content was determined according to the standard technique without sample tilt.

The data in the table shows that with all modes of the ion-plasma treatment the processes of enrichment of the crystal surface with metal atoms are observed. At the same time, the higher is ion energy and the longer is time of the process, the more explicit is the enrichment with gallium. To explain this result, it is necessary to consider two simultaneously running processes: the preferential sputtering of tellurium in the process of plasma treatment and the repeated deposition of gallium onto the surface in the working zone of the reactor.

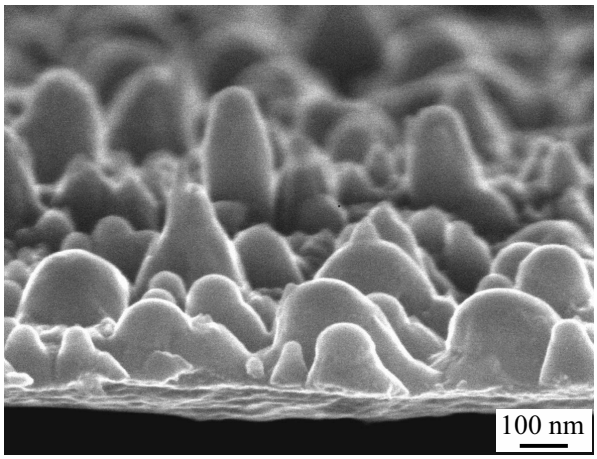

Figure 2. SEM-image of vertical cleavage of the gallium telluride crystal with large semi-spherical drops and cone-shaped structures between them. $E_i = 200$ eV, $t = 60$ s (*type C*).

Within the framework of linear cascade theory [37] the ratio of partial sputtering yields Y_{Te}/Y_{Ga} is determined by their surface concentration N^S_{Te}, N^S_{Ga}, surface binding energy U_{Te}, U_{Ga}, masses M_{Te} and M_{Ga}:

$$\frac{Y_{Te}}{Y_{Ga}} \simeq \frac{N^S_{Te}}{N^S_{Ga}} \left(\frac{M_{Ga}}{M_{Te}}\right)^{2m} \left(\frac{U_{Ga}}{U_{Te}}\right)^{1-2m},$$

where m in the conditions of our experiment on the basis of [37] can be taken equal to zero. For the calculations the sublimation energies of 131.6 kJ/mol (Te) and 277 kJ/mol (Ga) from [38] have been used. The evaluations have shown that $Y_{Te}/Y_{Ga} \approx 2.1$, which results in the preferential sputtering of tellurium. In addition, some of the tellurium released from the crystal due to its high volatility leaves the reactor's working zone, which results in the situation when gallium atoms take a more active participation in the repeated deposition onto the sputtered surface as compared with the chalcogen atoms. As a result of these two processes gallium atoms can form metal nanoparticles that are in the liquid state during the plasma treatment and play a major role in the formation of structures with various architectures on the gallium telluride surface.

Let us consider in more detail, as an example, the character of metal and chalcogen distribution on the surface of GaTe crystals after the drops are formed (*type C*). Fig. 3 shows a map of distribution of chemical elements on a surface section after the plasma treatment, in the right bottom corner for comparison a section of initial surface is left, which was masked in the process of sputtering. Red areas show places with increased gallium content. It follows from Fig. 3 that large drops on the surface (left part of the figure) correlate with red areas in the right part. The local determination of chemical composition for a large drop the area (point 1) and the initial surface (point 2) has shown that in point 2 the ratio of metal and chalcogen atoms is typical for the initial surface (Ga/Te = 1.12), and in point 1 the object in the form of a large drop (500 nm) is in fact a metal object (Ga/Te = 6.03).

Fig. 4 for the *type C* structure shows additionally a profile of gallium and tellurium distribution for cone-shaped structures located between large drops. The investigations were carried out on a vertical cleavage of the structure along the line starting at tops of small drops (diameter of ~ 100 nm) and penetrating into the crystal body. The analysis of Fig. 4 is indicative of the fact that maximum content of gallium and minimum amount of tellurium is typical for the region of nanodrop. In the region of cone the quantity of metal decreases gradually from the top to the base, and the quantity of chalcogen increases up to levels typical for the crystal body.

Results of the experiments described in this section confirm the general trend of enrichment of the structured surface of gallium telluride crystal with the metal under the plasma treatment. Depending on the ion energy and duration of the sputtering process that determine the surface temperature and the amount of the sputtered

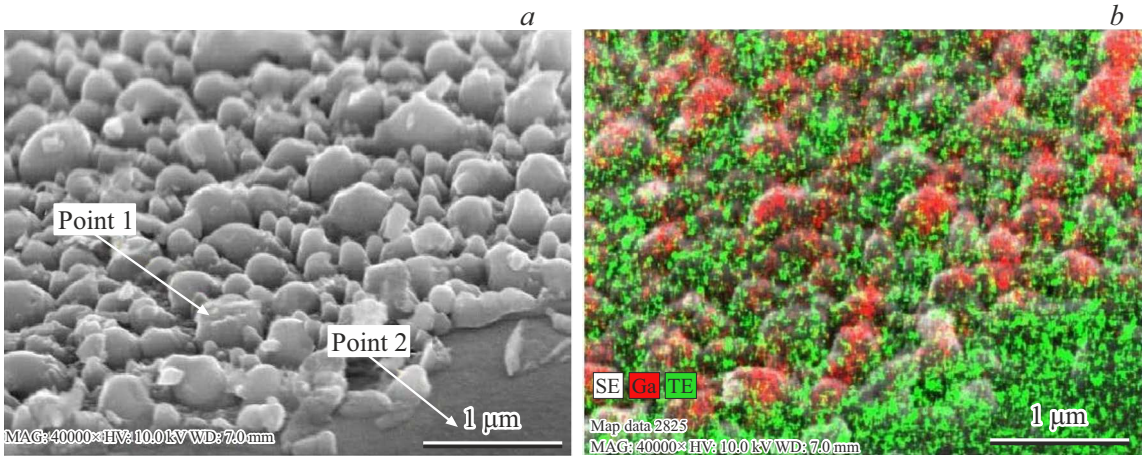

Figure 3. Mapping of the area of GaTe crystal surface that contains drops on the surface. $E_i = 200$ eV, $t = 60$ s (*type C*).

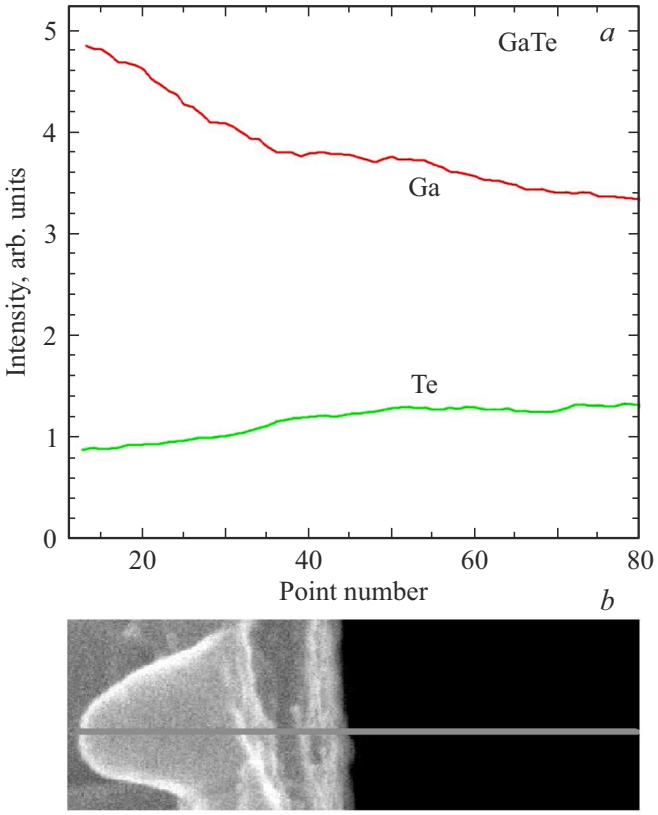

Figure 4. *a* — profile of gallium and tellurium distribution over the line running along the cone-shaped structure on the vertical cleavage of the crystal (*type C*, $E_i = 200$ eV, $t = 60$ s). *b* — image of the studied structure and the line of observation. Black region is the region of GaTe crystal.

material in the working zone, a number of scenarios are possible for the surface modification. Atoms of metal on the surface due to diffusion processes start to form nanoparticles, which in the case of gallium with its low melting temperature (302.9 K) are quickly transformed to the liquid state. The formed liquid nanodrops can play the role of metal-catalyst in the growth of nanostructures by the vapor–liquid–crystal (VLC) mechanism, which results in the formation of vertical nanocones and cone-shaped structures. A similar situation has been described by us for the plasma nanostructuring of $CuIn_{1-x}Ga_xSe_2$ films in [35]. The application of VLC mechanism to explain the growth of gallium telluride nanostructures is described in [31,39]. In addition, liquid drops of gallium can play the role of masks in the process of ion etching, which also promotes the formation of nanohillocks and nanocones. In the case of high etching rates and long times of treatment, due to the fusion of liquid drops the occurrence of large metal drops on the surface becomes the definitive process. Similar results regarding the formation of metal drops have been obtained by us for the plasma treatment of In_2S_3 films [36] that contain metal indium with a low melting temperature (429.7 K).

3.3. X-ray diffractometry investigations

Fig. 5 shows diffraction pattern of GaTe crystal in the initial state. The analysis of the diffraction pattern shows that the basis is formed by 6 intensive peaks referred to (−2 0 1), (−4 0 2), (−6 0 3), (−8 0 4), (−10 0 5) and (−12 0 6) lattice planes of the gallium telluride in the monoclinic phase. A similar pattern has been described earlier in [10] for GaTe crystals grown by the method of vertical zone-melting followed by a long-term storing or annealing, and for the crystals produced by Bridgman method [40]. The (−2 0 1) planes coincide with the planes along which the break of Van der Waals bonds takes place and the crystal is split into separate plates when cleaving normally to the direction of growth. In addition, the diffraction pattern (Fig. 6) shows scarce weak reflections referred to inclusions of gallium telluride with monoclinic structure with other directions of planes (ICDD PDF-2 2020 01-074-8974) and gallium telluride with a hexagonal structure (ICDD PDF-2 2020 01-089-2675).

After the ion-plasma treatment in all modes, no significant changes in the main six peaks of GaTe have been observed. Changes related to the appearance of new peaks or disappearance of initial peaks have been observed only among the low-intensity peaks (Fig. 7). A general feature for all modes of plasma treatment has been the appearance of nanostructured gallium on the crystal surface. It is known [41,42] that in the case of small sizes of gallium crystallites metal nanoparticles can be in different structure modifications and, as a consequence, the X-ray diffraction patterns do not coincide with classical diffraction patterns for the bulk state. In the scope of this study, the analysis of changes in diffraction patterns is performed taking into account the polymorphism of gallium nanoparticles. The appearance of new experimental peaks in all treatment modes correspond to the formation of gallium nanostructures with a tetragonal body-centered lattice with constant

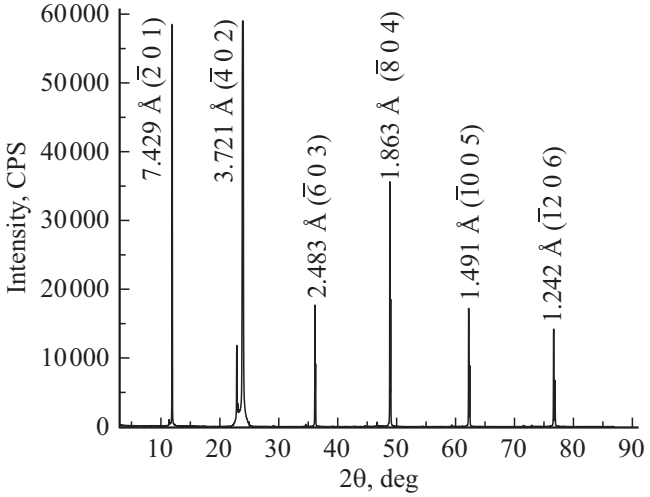

Figure 5. Diffraction pattern of the GaTe crystal in the initial state. The figure shows interplanar distances and Miller indices for the GaTe with monoclinic structure (01-074-8974).

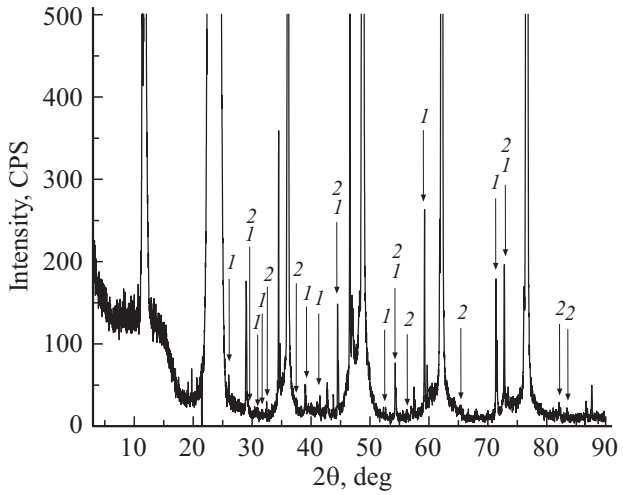

Figure 6. Fragment of diffraction pattern of the initial GaTe crystal in the intensity range of 0–500 CPS. Numbers show maxima of intensity of diffraction peaks for the following compounds: *1* — GaTe with monoclinic structure (01-074-8974); *2* — GaTe with hexagonal structure (01-089-2675).

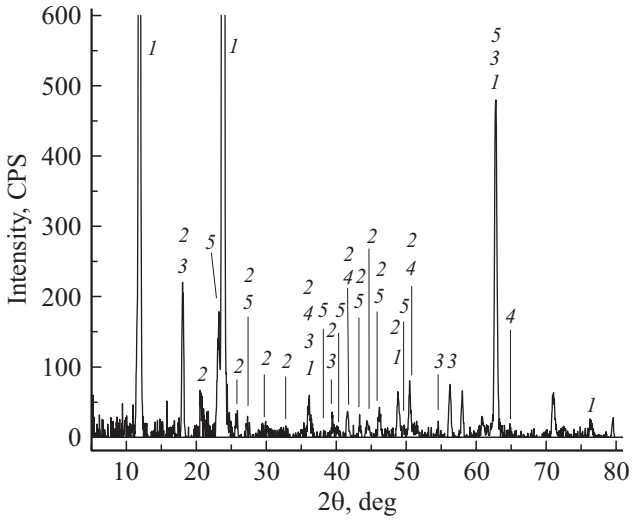

Figure 7. Fragment of diffraction pattern of the GaTe crystal after plasma treatment in the intensity range of 0–600 CPS. Numbers show maxima of intensity of diffraction peaks for the following compounds: *1* — textured GaTe with monoclinic structure (01-074-8974); *2* — polycrystalline GaTe with monoclinic structure (01-074-8974); *3* — Ga with tetragonal structure with cell parameters $a = b = 3.25$ Å, $c = 4.95$ Å [41]; *4* — Ga_2O_3 with rhombohedral structure (00-006-0503); *5* — Te with hexagonal structure (01-079-0736).

$a = b = 0.325$ nm, $c = 0.495$ nm [41]. The diffraction patterns show peaks corresponding to (1 0 1), (0 0 2), (1 1 0), (1 1 2), (2 0 0), (1 0 3), (1 2 1), (2 0 2) planes of such structure modification of gallium. In addition, on the surface of gallium telluride after plasma treatment low intensity peaks are observed from γ-Ga_2O_3 (ICDD PDF-2 2020 01-082-3194), from crystalline TeO_2 (00-042-1365, 01-074-1131) and from tellurium with hexagonal structure (01-079-0736). The appearance of Ga_2O_3 in this case may be related to the partial oxidation of the gallium drops being formed on the crystal surface.

3.4. Raman scattering spectra

To gain additional information on the effect of treatment in Ar plasma on the structure of GaTe surface, RS spectra were measured (Fig. 8). As can be seen from Fig. 8, the RS spectrum of the initial surface has the most intensive peaks at ~ 125 and $\sim 141\,cm^{-1}$ not typical for GaTe, which presence according to [3] and [43] is indicative of a significant content of chemisorbed oxygen on the surface. Peaks in this spectral region are typical also for the following types of oxides: α-TeO_2, Te_4O_9, β-Ga_2O_3 [44–46], however, except for the indicated line the RS spectra of oxides should have a number of peaks in the range of $300–800\,cm^{-1}$, which are absent in our case (insert to Fig. 8). For the *type A* surface the intensity of peaks at 125 and $141\,cm^{-1}$ is approximately 1.6 times les in relation to their intensity in the RS spectra of the initial sample. Along with peaks at 125 and $141\,cm^{-1}$, in RS spectra of the *type A* surface low-intensity peaks are observed, which are typical for the crystalline GaTe — A_g (66, 76, 109, 115, 152, 178, 209, 269–271, $283–284\,cm^{-1}$), B_g (56–58, 163–164, $170\,cm^{-1}$) and B_u ($90\,cm^{-1}$) [3,47,48]. For the *type B* surface the intensity of peaks at 125 and $141\,cm^{-1}$ in RS spectra is approximately 3 times less as compared with their intensity in RS spectra of the initials sample. Especially explicit is the suppression of peaks at 125 and $141\,cm^{-1}$ for the *type C* surface: their intensity is decreased by approximately 18 times. Such an effect may be related to the tellurium depletion of the GaTe surface and its enrichment with gallium, which impedes the chemisorption of oxygen on tellurium. The decrease in intensity of RS peaks at 125 and $141\,cm^{-1}$ with the transition from *type A* surface to

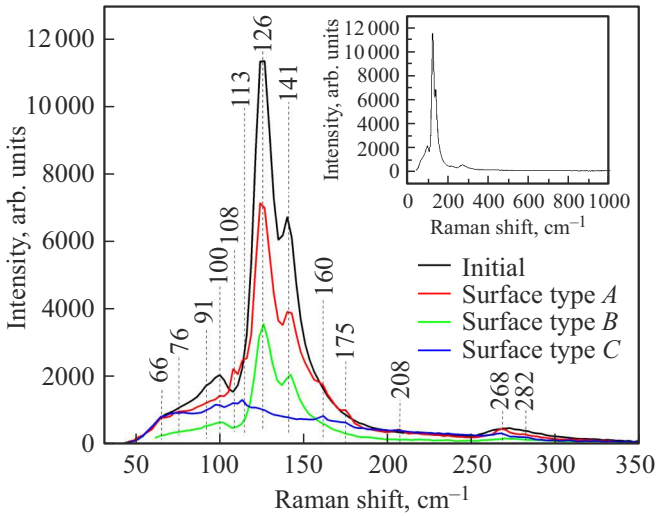

Figure 8. Raman scattering spectra of GaTe crystal surfaces. The insert shows spectrum in an extended frequency range.

type C surface correlates with the change in the oxygen content shown in the table.

3.5. Optical reflection spectra

Spectral response of specular reflection factor (R) of the initial surface of GaTe crystals in the range of incident radiation energy of 0.4−6.2 eV is shown in Fig. 9. The reflection spectrum of the initial GaTe surface has no clearly defined energy structure, however, two features in the form of local minima near 0.76 and 1.52 eV, as well as a minimum near 4.5 eV are distinguished. In terms of energy position, the local minimum near 0.76 eV can be associated with the edge of optical absorption with indirect transitions to GaTe-O_2 [3] formed on the surface due to the chemisorption of oxygen by tellurium. The energy position of the local minimum near 1.52 eV corresponds to the blurred fundamental absorption edge [49,50]. A wide unsymmetrical minimum in the region of 4.5 eV is typical for the surface of GaTe crystals and probably is formed by a combination of interband transitions between the filled valence band π and the empty conduction band π_4 [50].

The nanostructuring of the surface of GaTe crystals in argon plasma in fact has resulted in complete suppression of the specular optical reflection (Fig. 9): the specular reflection factor throughout the entire studied spectral range is not more than 2% for the produced types of surfaces (*types A, B* and *C*). Fig. 9 shows the specular reflection spectrum for the *type A* surface, the reflection factor for *type B* and *type C* surfaces is not higher than that for the *type A* surface. A similar effect has been described in [51]: plasma nanostructuring of pyrolytic graphite has resulted in appearance of nanostructures (nanocolumns, nanodiscs, nanocones) on the surface and decrease in the average specular reflection factor in the range of 400−2000 nm c 30−60% down to $0.05 \pm 0.03\%$. The detected effect may be indicative of the formation of nanostructures on the surface of GaTe crystals, which are strongly scattering and/or absorbing centers.

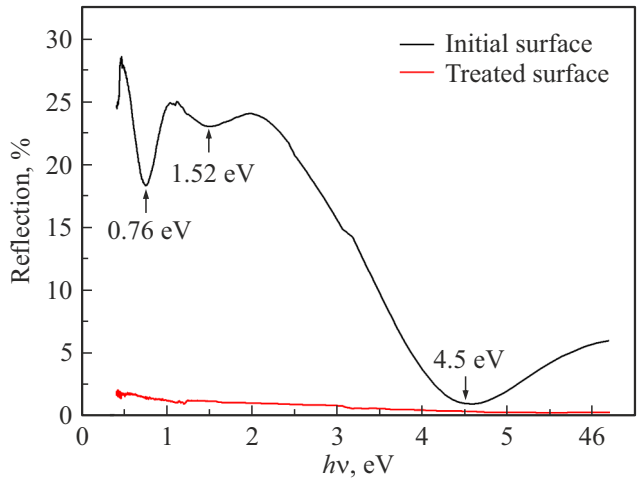

Figure 9. Optical reflection spectra of GaTe crystal surface for the initial state (top curve) and after the plasma treatment with $E_i = 100$ eV, $t = 120$ s (*type A*).

4. Conclusion

Results of this study have shown that the treatment of gallium telluride crystals in high-density argon plasma of low-pressure high-frequency induction discharge results in an effective modification of the surface with formation of nanostructures and submicron structures with different architectures. With variation of argon ion energy (100−200 eV) and treatment time (15−120 s) a targeted creation of ensembles of nanohillocks, nanocones, drop structures is possible. It is worth to note that processes of sputtering are accompanied by a decrease in tellurium concentration in the near-surface layer of crystal, which promotes the decrease in oxidation processes in the air atmosphere and results in the decrease in the concentration of oxygen on the surface. In the process of ion-plasma treatment an active enrichment of the crystal surface with gallium with formation of nanoscale and submicron drops of metal has been observed. An important practical result of the nanostructuring of GaTe crystal surface is the detected effect of suppression of specular optical reflection, which can be used in instrument optoelectronic systems based on gallium telluride.

Funding

This study was carried out under the state assignment of Valiev IPT RAS, project No. FFNN-2022-0017; the state assignment of Osipyan ISSP RAS, project FFWE-2022-0003; within the scope initiative R & D activity of Yaroslavl State University and the State Research Program of the Republic of Belarus „Material science, new materials and technologies“ (1.4.2). SEM-studies and X-ray diffractometry studies are carried out in the Center of Equipment Sharing „Diagnostics of microstructures and nanostructures“ under financial support from the Ministry of Education and Science of the Russian Federation.

Conflict of interest

The authors declare that they have no conflict of interest.

References

[1] A. Yamamoto, A. Syouji, T. Goto, E. Kulatov, K. Ohno, Y. Kawazoe, K. Uchida, N. Miura. Phys. Rev. B: Condens. Matter. **64**, *3*, 035210 (2001).
[2] M. Liu, S. Yang, M. Han, S. Feng, G.G. Wang, L. Dang, B. Zou, Y. Cai, H. Sun, J. Yu, J.C. Han, Z. Liu. Small **17**, *21*, 2007909 (2021).
[3] J.J. Fonseca, S. Tongay, M. Topsakal, A.R. Chew, A.J. Lin, C. Ko, A.V. Luce, A. Salleo, J. Wu, O. Dubon. Adv. Mater. **28**, *30*, 6465 (2016).
[4] J. Susoma, J. Lahtinen, M. Kim, J. Riikonen, H. Lipsanen. AIP Adv. **7**, *1*, 015014 (2017).

[5] Q. Chen, Y. Chen, J. Wang, M. Liu, Z. Chen. Crystals **12**, *5*, 627 (2022).
[6] T. Singha, M. Karmakar, P. Kumbhakar, C.S. Tiwary, P.K. Datta. Appl. Phys. Lett. **120**, *2*, 021101 (2022).
[7] A.V. Kosobutsky, S.Yu. Sarkisov. Phys. Solid State **60**, *9*, 1686 (2018).
[8] K. Lai, S. Ju, H. Zhu, H. Wang, H. Wu, B. Yang, E. Zhang, M. Yang, F. Li, S. Cui, X. Deng, Z. Han, M. Zhu, J. Dai. Commun. Phys. **5**, 143 (2022).
[9] J.F. Sánchez-Royo, J. Pellicer-Porres, A. Segura, V. Muñoz-Sanjosé, G. Tobías, P. Ordejón, E. Canadell, Y. Huttel. Phys. Rev. B **65**, *11*, 115201 (2002).
[10] N.N. Kolesnikov, E.B. Borisenko, D.N. Borisenko, A.V. Timonina. J. Cryst. Growth **365**, *1*, 59 (2013).
[11] Q. Zhao, T. Wang, Y. Miao, F. Ma, Y. Xie, X. Ma, Y. Gu, J. Li, J. He, B. Chen, S. Xi, L. Xu, H. Zhen, Z. Yin, J. Li, J. Ren, W. Jie. Phys. Chem. Chem. Phys. **18**, 18719 (2016).
[12] Xi. Wang, Xu. Wang, H. Zou, Y. Fu, X. He, L. Zhang. Chin. Phys. B **30**, *1*, 01640 (2021).
[13] Y.W. Yu, M. Ran, S.S. Zhou, R.Y. Wang, F.Y. Zhou, H.Q. Li, L. Gan, M.Q. Zhu, T.Y. Zhai. Adv. Funct. Mater. **29**, *23*, 1901012 (2019).
[14] L. Gouskov, A. Gouskov. Phys. Status Solidi **51**, K213 (1979).
[15] S. Huang, Y. Tatsumi, X. Ling, H. Guo, Z. Wang, G. Watson, A.A. Puretzky, D.B. Geohegan, J. Kong, J. Li, T. Yang, R. Saito, M.S. Dresselhaus. ACS Nano **10**, *9*, 8964 (2016).
[16] H. Wang, M. Chen, M. Zhu, Y. Wang, B. Dong, X. Sun, X. Zhang, S. Cao, X. Li, J. Huang, L. Zhang, W. Liu, D. Sun, Y. Ye, K. Song, J. Wang, Y. Han, T. Yang, H. Guo, C. Qin, L. Xiao, J. Zhang, J. Chen, Z. Han, Z. Zhang. Nature Commun. **10**, 2302 (2019).
[17] F. Liu, H. Shimotani, H. Shang, T. Kanagasekaran, V. Zólyomi, N. Drummond, V.I. Fal'ko, K. Tanigaki. ACS Nano **8**, *1*, 752 (2014).
[18] K.C. Mandal, R.M. Krishna, T.C. Hayes, P.G. Muzykov, S. Das, T.S. Sudarshan. In IEEE Nucl. Sci. Symp. **58**, *4*, 3719 (2010). DOI:10.1109/NSSMIC.2010.5874507
[19] X. Xia, X. Li, H. Wang. J. Semicond. **41**, 072902 (2020).
[20] Z. Wang, K. Xu, Y. Li, X. Zhan, M. Safdar, Q. Wang, F. Wang, J. He. ACS Nano **8**, *5*, 4859 (2014).
[21] P. Hu, J. Zhang, M. Yoon, X.-F. Qiao, X. Zhang, W. Feng, P. Tan, W. Zheng, J. Liu, X. Wang, J. Idrobo, D. Geohegan, K. Xiao. Nano Res. **7**, *5*, 694 (2014).
[22] D.N. Bose, S. Pal. Phys. Rev. B: Condens. Matter Mater. Phys. **63**, *23*, 235321 (2001).
[23] S. Pal, D. Bose. Solid State Commun. **97**, *8*, 725 (1996).
[24] S. Siddique, C.C. Gowda, R. Tromer, S. Demiss, A.R. Singh Gautam, O.E. Femi, P. Kumbhakar, D.S. Galvao, A. Chandra, C.S. Tiwary. ACS Appl. Nano Mater. **4**, *5*, 4829 (2021).
[25] L.-C. Tien, Y.-C. Shih. Nanomaterials **11**, *3*, 778 (2021).
[26] F. Bondino, S. Duman, S. Nappini, G. D'Olimpio, C. Ghica, T.O. Menteş, F. Mazzola, M.C. Istrate, M. Jugovac, M. Vorokhta, S. Santoro, B. Gürbulak, A. Locatelli, D.W. Boukhvalov, A. Politano. Adv. Funct. Mater. **32**, *41*, 2205923 (2022).
[27] V.P. Hoang Huy, I.T. Kim, J. Hur. Nanomaterials **12**, *19*, 3362 (2022).
[28] G. Yu, Z. Liu, X.M. Xie, X. Ouyang, G.Z. Shen. J. Mater. Chem. C **2**, *30*, 6104 (2014).
[29] H. Cai, B. Chen, G. Wang, E. Soignard, A. Khosravi, M. Manca, X. Marie, S. L.Y. Chang, B. Urbaszek, S. Tongay. Adv. Mater. **29**, *8*, 1605551 (2017).
[30] L.-C. Tien, Y.-C. Shih, C.-Y. Chen, Y.-T. Huang, R.-S. Chen. J. Alloys Comp. **876**, 160195 (2021).
[31] S.P. Saeb, M. Varga. In: ASDAM 2022 / Eds J. Marek et al. IEEE 2022, 111-113 (2022). ISBN 978-1-6654-6977-7.
[32] I. Levchenko, K. Ostrikov. J. Phys. D **40**, *8*, 2308 (2007).
[33] S. Zimin, E. Gorlachev, I. Amirov. Inductively Coupled Plasma Sputtering: Structure of IV−VI Semiconductors. In: Encyclopedia of Plasma Technology. 1st ed. CRC Press, N.Y. (2017) P. 679−691. https://doi.org/10.1081/E-EPLT-120053966 https://www.routledgehandbooks.com/doi/10.1081/E-EPLT-120053966
[34] S.P. Zimin, E.S. Gorlachev, I.I. Amirov, V.V. Naumov, R. Juskenas, M. Skapas, E. Abramof, P.H.O. Rappl. Semicond. Sci. Technol. **34**, *9*, 095001 (2019).
[35] S.P. Zimin, E.S. Gorlachev, D.A. Mokrov, I.I. Amirov, V.V. Naumov, V.F. Gremenok, R. Juskenas, M. Skapas, W.Y. Kim, K. Bente, Y.-D. Chung. Semicond. Sci. Technol. **32**, *7*, 075014 (2017).
[36] S. Rasool, K. Saritha, K.T. Ramakrishna Reddy, M.S. Tivanov, V.F. Gremenok, S.P. Zimin, A.S. Pipkova, L.A. Mazaletskiy, I.I. Amirov. Mater. Res. Exp. **7**, *1*, 016431 (2020).
[37] P. Sigmund. Elements of sputtering theory. In: Nanofabrication by Ion-Beam Sputtering / Eds T. Som, D. Kanjilal. Pan Stanford Publishing (2013). P. 1−40. https://doi.org/10.4032/9789814303767
[38] D.R. Lide. CRC Handbook of Chemistry and Physics. 76th ed. CRC Press, N.Y. (1995) P. 3−320.
[39] T. Li, J. Feng, L. Liang, W. Sun, X. Wang, J. Wu, P. Xu, M. Liu, D. Ma. ACS Omega **5**, *16*, 9550 (2020).
[40] J. Dong, K.-P. Gradwohl, Y. Xu, T. Wang, B. Zhang, B. Xiao, C. Teichert, W. Jie. Photon. Res. **7**, *5*, 518 (2019).
[41] I.G. Sorina, C. Tien, E.V. Charnaya, Yu.A. Kumzerov, L.A. Smirnov. Phys. Solid State **40**, *8*, 1407 (1998).
[42] M. Yarema, M. Wörle, M.D. Rossell, R. Erni, R. Caputo, L. Protesescu, K.V. Kravchyk, D.N. Dirin, K. Lienau, F. Rohr, A. Schilling, M. Nachtegaal, M.V. Kovalenko. J. Am.Chem. Soc. **136**, *35*, 12422 (2014).
[43] M. Kotha, T. Murray, D. Tuschel, S. Gallis. Nanomaterials **9**, *11*, 1510 (2019).
[44] J.C. Champarnaud-Mesjard, S. Blanchandin, P. Thomas, A. Mirgorodsky, T. Merle-Méjean, B. Frit. J. Phys. Chem. Solids **61**, *9*, 1499 (2000).
[45] M. Smirnov, V. Kuznetsov, E. Roginskii, J. Cornette, M. Dutreilh-Colas, O. Noguera, O. Masson, P. Thomas. J. Phys.: Condens.Matter. **30**, *47*, 475403 (2018).
[46] B.M. Janzen, P. Mazzolini, R. Gillen, A. Falkenstein, M. Martin, H. Tornatzky, J. Maultzsch, O. Bierwagen, M.R. Wagner. J. Mater. Chem. C. **9**, *7*, 2311 (2021).
[47] N.T. Hoang, J.H. Lee, T.H. Vu, S. Cho, M.J. Seong. Sci. Rep. **11**, 21202 (2021).
[48] J.C. Irwin, B.P. Clayman, D.G. Mead. Phys. Rev. B **19**, *4*, 2099 (1979).
[49] C. Tatsuyama, Y. Watanabe, C. Hamaguchi, J. Nakai. J. Phys. Soc. Jpn **29**, *1*, 150 (1970).
[50] V. Grasso, G. Mondio, G. Saitta. Phys. Lett. A **46**, *2*, 95 (1973).
[51] Y. Sun, J. Evans, F. Ding, N. Liu, W. Liu, Y. Zhang, S. He. Opt. Exp. **23**, *15*, 20115 (2015).